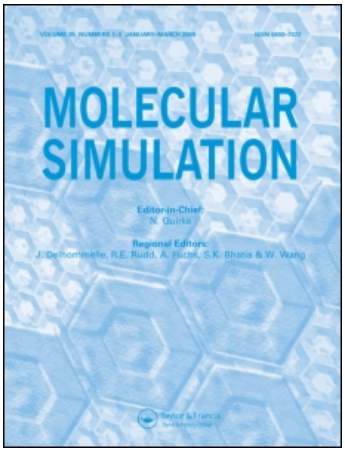

Molecular Simulation
Publication details, including instructions for authors and subscription information:
http://www.informaworld.com/smpp/title~content=t713644482

Formation of Spherical Micelles in a supercritical Solvent: Lattice Monte Carlo Simulation and Multicomponent Solution Model

Martin LÍsal[a]; Carol K. Hall[a]; Keith E. Gubbins[a]; Athanassios Z. Panagiotopoulos[b]
[a] Department of Chemical Engineering, North Carolina State University, Raleigh, NC, USA [b] Department of Chemical Engineering, Princeton University, Princeton, NJ, USA

Online publication date: 26 October 2010

To cite this Article LÍsal, Martin , Hall, Carol K. , Gubbins, Keith E. and Panagiotopoulos, Athanassios Z.(2003) 'Formation of Spherical Micelles in a supercritical Solvent: Lattice Monte Carlo Simulation and Multicomponent Solution Model', Molecular Simulation, 29: 2, 139 — 157
To link to this Article: DOI: 10.1080/0892702031000065809
URL: http://dx.doi.org/10.1080/0892702031000065809

Molecular Simulation, 2003 Vol. 29 (2), pp. 139–157

Formation of Spherical Micelles in a supercritical Solvent: Lattice Monte Carlo Simulation and Multicomponent Solution Model

MARTIN LÍSAL[a,*], CAROL K. HALL[a], KEITH E. GUBBINS[a] and ATHANASSIOS Z. PANAGIOTOPOULOS[b]

[a]*Department of Chemical Engineering, North Carolina State University, Raleigh, NC 27695-7905, USA*
[b]*Department of Chemical Engineering, Princeton University, Princeton, NJ 08544-5263, USA*

(Received September 2001; accepted in final form September 2001)

We modify Larson's lattice model [Larson, R.G., Scriven, L.E. and Davis, H.T. (1985). *J. Chem. Phys.*, 83, 2411–2420] and use it to study formation of spherical micelles in a supercritical solvent by large-scale Monte Carlo (MC) simulations and by the multicomponent solution model. Carbon dioxide and perfluoroalkylpoly(ethylene oxide) serve as prototypes for the solvent and surfactant, respectively. Larson-model type parameters for carbon dioxide and perfluoroalkylpoly(ethylene oxide) are obtained using experimental values of critical parameters and solubility along with a modified Berthelot combining rule. We perform canonical MC simulations at a supercritical temperature and low surfactant concentrations, varying the number of surfactant head and tail segments and the solvent density. Various properties such as the critical micelle concentration, the aggregate size distribution and the size of the micelles is evaluated. The multicomponent solution model and the simulation results for the aggregate size distribution are then combined to determine the standard state chemical potential for the spherical micelles and the intermicellar interaction; we present a novel approach to model this standard state chemical potential. The implications of these results for the thermodynamics of the formation of the spherical micelles in supercritical solvents are explored.

Keywords: Lattice model of supercritical solvent–surfactant systems; Multicomponent solution model; Spherical micelles; Thermodynamics

INTRODUCTION

Supercritical fluids are becoming increasingly important solvents in polymer science and engineering [1,2]. Supercritical carbon dioxide ($scCO_2$), in particular, is a widely used solvent due to its low cost, moderate critical conditions ($T_C = 304.13\,K$, $P_C = 73.773\,bar$), and environmentally benign nature. However, several important classes of substances such as water, hydrophilic substances and most polymers exhibit very low solubility in $scCO_2$. This has led to an extensive search for surfactants with the ability to solubilize such substances in $scCO_2$ [3]. Surfactant molecules used in $scCO_2$ have two mutually incompatible components: a CO_2 philic tail with an affinity for CO_2 molecules and a CO_2-phobic head with a repulsion to CO_2 molecules. When immersed in $scCO_2$ these surfactants self-assemble and form micelles with the CO_2-phobic head in the core. These micelles can be employed to enhance the solubility of normally insoluble compounds by incorporating them into their core, a process known as *micellar solubilization*.

A common feature of the surfactants used in $scCO_2$ is that they contain tails with fluorinated (CF_3, CF_2) segments. The properties of fluorinated compounds are distinctly different from those of their hydrocarbon analog due to their relatively large size and the highly electronegative nature of the fluorine atom [4]. This is manifested, for example, by the high solubility of fluorocarbons in $scCO_2$, in contrast to the low solubility found for their hydrocarbon analog [5].

During the last decade, there has been a huge experimental effort devoted to the study of the formation of micelles in $scCO_2$ [3]. In comparison there have been only a few attempts to use

*Corresponding author. Address: E. Hála Laboratory of Thermodynamics, Institute of Chemical Process Fundamentals, Academy of Sciences of the Czech Republic, 165 02 Prague 6, Czech Republic.

ISSN 0892-7022 print/ISSN 1029-0435 online © 2003 Taylor & Francis Ltd
DOI: 10.1080/0892702031000065809

molecular-level approaches to understand the process of micellization in $scCO_2$. Salaniwal *et al.* [6–8] studied self-assembly of micelles in $scCO_2$-dichain surfactant–water systems by molecular dynamics simulations with an atomistic model. Baysal *et al.* [9] performed molecular dynamics calculations with an atomistic model to study the conformational properties of single chain diblocks of poly(1,1-dihydroperfluorooctyl acrylate) and poly(vinyl acetate) in $scCO_2$. Luna-Bárcenas *et al.* [10] used the statistical associating fluid theory [11] to model the phase behavior of $scCO_2$–poly(FOA) systems and Colina *et al.* [12] combined the osmotic pressure approach with the statistical associating fluid theory to study phase diagrams of copolymers in $scCO_2$.

The time-scale for the assembly of equilibrium surfactant structures is currently beyond the reach of atomistic simulations for many surfactant solutions of interest. This has led to the introduction of coarse-grained models in which a number of atoms are grouped together and are represented in a simplified manner. The two main families of coarse-grained models employed are off-lattice models and lattice models. The former are typically more versatile and realistic while the latter are usually more computationally efficient [13]. Larson's model of water–amphiphile–oil systems [14] is typical of the many lattice models available. It uses a fully occupied cubic lattice with lattice points representing a solvent molecule, a solute molecule or a surfactant segment. An entity on a given lattice point interacts with the nearest neighbor and diagonally nearest neighbor points, resulting in a coordination number of 26. No interactions at greater distances are included in the model. Larson's model simplifies molecular interactions in water–amphiphile–oil systems by assuming that the contact energies of lyophilic and hydrophilic units are the same regardless of which of the lyophilic units (tail or oil), or which of the hydrophilic units (head or water) are interacting. Monte Carlo (MC) simulations conducted on Larson's model have been able to qualitatively describe different phases in water–amphiphile–oil systems [15].

The objective of this work is to study formation of spherical micelles in a supercritical solvent by large-scale MC simulations and by the multicomponent solution model on a modified version of Larson's lattice model. We use carbon dioxide and perfluoroalkylpoly(ethylene oxide) as prototypes for the solvent and surfactant, respectively. We chose perfluoroalkylpoly(ethylene oxide): $F(CF_2)_n(CH_2CH_2O)_mH$ ($m = 4–9$, $n = 7–11$; $m < n$) as the prototypical nonionic surfactant because: (i) it is linear and easy to model; (ii) it has a CO_2-philic tail, $F(CF_2)_n$; and (iii) its head, $(CH_2CH_2O)_mH$, interacts favorably with water molecules. Moreover, Fulton *et al.* [16] have already shown that this surfactant forms micelles in $scCO_2$.

In the remainder of this paper, we first introduce a modified version of Larson's model (second section) and show how to estimate Larson-model type parameters for carbon dioxide and perfluoroalkyl-poly(ethylene oxide) (third section). This is followed by a description of the simulation methodology and by the definitions of several quantities that characterize the micellization process (fourth section). The fifth section describes the multicomponent solution model. Then, we present a novel approach to model the standard state chemical potential for spherical micelles (sixth section). The seventh section presents and discusses the results for the critical micelle concentration (cmc), the aggregate size distribution, the size of the micelles, the standard state chemical potential for the spherical micelles and the intermicellar interaction. We conclude with a summary in the eighth section.

MODEL

Our lattice model is a modification of Larson's model [14] which treats a supercritical solvent–surfactant system as a binary mixture of N_s monomer solvent molecules (CO_2, denoted by s), occupying one lattice point each, and N_A surfactant chain molecules occupying r lattice points each on a lattice with coordination number $z = 26$. We denote the surfactant as H_mT_n, where H stands for a head segment (either a CH_2CH_2O or a CH_2CH_2OH group) and T for a tail segment (either a CF_2 or a CF_3 group); therefore $r = m + n$.

In contrast to Larson's model, our lattice is not fully occupied but instead contains N_v vacancies (v). This allows us to study micellar behavior as a function of the solvent density. Each molecular unit (s, T and H) interacts with the other molecular units with a contact energy ε_{ab} $(a, b = s, T, H)$. Negative values of ε_{ab} correspond to attractive interactions while nonnegative values of ε_{ab} represent repulsive interactions. It should also be mentioned that the vacancies are treated as molecular units in our model with ε_{vb} $(b = s, T, H, v)$ equal to zero by definition [17].

When dealing with mixtures and their properties, the real interest is in the thermodynamic functions of mixing, i.e. in the values of functions relative to their values for the pure fluids. The thermodynamic mixing functions such as the free energy of mixing depend on the interchange energies, w_{ab}, which are linear combinations of contact energies [18] as:

$$w_{ab} = \varepsilon_{ab} - \frac{\varepsilon_{aa} + \varepsilon_{bb}}{2} \qquad (a, b = s, T, H, v \text{ with } a \neq b) \tag{1}$$

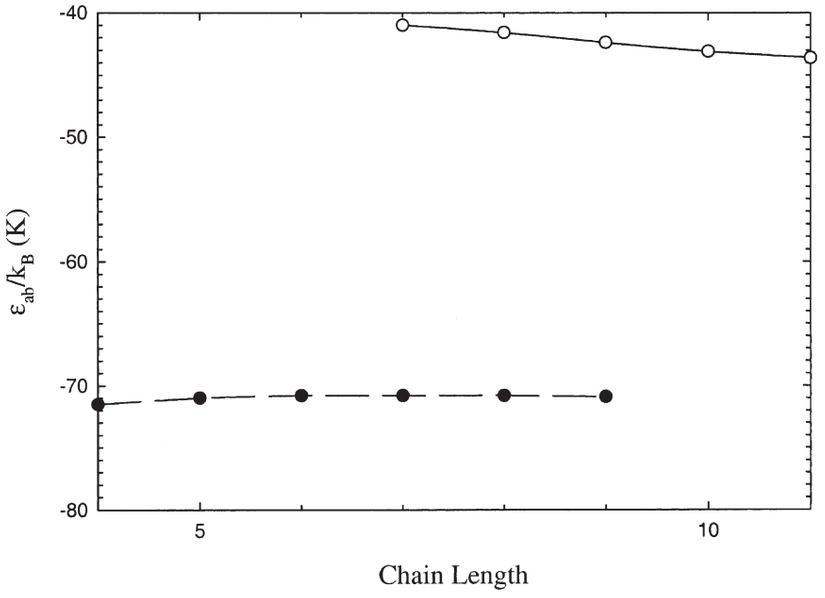

FIGURE 1 The surfactant tail–tail (○,—) and head–head (•, – – –) segment contact energies ε_{ab}/k_B for different chain lengths; k_B is Boltzmann's constant.

Instead of w_{ab}, lattice fluid theories usually employ the Flory–Huggins interaction parameters, χ_{ab}, [19] defined to be

$$\chi_{ab} = \frac{z}{k_B T} w_{ab} \quad (a, b = s, T, H, v \text{ with } a \neq b) \qquad (2)$$

where T is the temperature and k_B is Boltzmann's constant.

PARAMETER ESTIMATION

Like Contact Energies

The contact energies between like molecular units are obtained by matching the critical temperatures of the model fluids with the critical temperatures of the real fluids. A monomer on a lattice with coordination number $z = 26$ is the model fluid for carbon dioxide. For the nonionic surfactant, $F(CF_2)_n(CH_2CH_2O)_mH$ ($m = 4$–9, $n = 7$–11; $m < n$), we consider the tail and head interactions separately and make the usual assumption that the interaction parameters of a particular molecular group can be transferred to different molecules [20]. The contact energies between tail–tail and head–head segments are found by matching the critical temperatures of chains of lengths n and m (on the lattice with $z = 26$) with the critical temperatures of C_nF_{2n+2} and $H(CH_2CH_2O)_mH$, respectively.

We utilize the following experimental values for the critical temperatures: $T_C = 304.13$ K for carbon dioxide and $\{(n, T_C)\} = \{(7, 475.3\,\text{K}), (8, 498.2\,\text{K}), (9, 521.2\,\text{K}), (10, 542.35\,\text{K}), (11, 559.2\,\text{K})\}$ for C_nF_{2n+2} [21]. Since the experimental critical temperatures for $H(CH_2CH_2O)_mH$ are not known, we estimate them by the Fedors group-contribution method [21]. The estimation gives: $\{(m, T_C)\} = \{(4, 713\,\text{K}), (5, 754\,\text{K}), (6, 790\,\text{K}), (7, 821\,\text{K}), (8, 848\,\text{K}), (9, 872\,\text{K})\}$. The critical temperatures of the model fluids are available from lattice Gibbs ensemble MC simulations [22]: $T_C^* \equiv k_B T_C / w_{av} = 11.7$ for monomers and $\{(r, T_C^*)\} = \{(4, 19.9), (5, 21.3), (6, 22.3), (7, 23.2), (8, 23.9), (9, 24.6), (10, 25.2), (11, 25.7)\}$ for chains of length r.

Comparing the T_C value for the monomer with that for pure CO_2 we find that the solvent–solvent (CO_2–CO_2) contact energy is: $\varepsilon_{ss}/k_B = -52$ K. The tail–tail and head–head segment contact energies obtained for different chain lengths are plotted in Fig. 1. Since they depend only slightly on the chain length we average them over the chain length to obtain final values for the tail–tail and head–head segment contact energies of $\varepsilon_{TT}/k_B = -42$ K and $\varepsilon_{HH}/k_B = -71$ K, respectively. All like contact energies are summarized in Table I.

TABLE I The contact energies ε_{ab}/k_B and the associated values of the Flory–Huggins interaction parameters χ_{ab} at a reduced temperature of 1.15 for the lattice model of supercritical solvent–surfactant systems studied; k_B is Boltzmann's constant

Like interactions		*Unlike interactions*		
Type of interaction	ε_{ab}/k_B (K)	*Type of interaction*	ε_{ab}/k_B (K)	χ_{ab}
Solvent–solvent	−52	Solvent–tail	−44	0.2
Tail–tail	−42	Solvent–head	0	4.6
Head–head	−71	Head–tail	−49	0.6

Unlike Contact Energies

The contact energies between the unlike molecular units cannot be obtained simply from the standard Berthelot combining rule [23], since this is for repulsion and dispersion interactions, whereas our contact energies include contributions from electrostatic and other forces. Its use would result in having large solubilities for surfactant head segments in $scCO_2$, in contrast to what is known empirically. Generally-speaking, the character and strength of the interactions between two components are established by the sign and magnitude of the Flory–Huggins interaction parameters χ_{ab} [24]. Negative values of χ_{ab} correspond to electrostatic or hydrogen bonding interactions between unlike species while small and positive values of χ_{ab} characterize dispersion interactions. For two mutually incompatible (insoluble) components χ_{ab} is generally large and positive (e.g. $\chi \approx 5$ for water–oil systems at room temperature) [24,25].

We use the following strategy for determining the unlike contact energies: (i) we adjust the contact energy between mutually incompatible molecular units [solvent–head segment (CO_2–CH_2CH_2O or CO_2–CH_2CH_2OH)] to roughly represent experimental solubility data, and (ii) we modify the standard Berthelot combining rule to reflect the character and strength of the interactions between the mutually compatible molecular units [solvent–tail segment (CO_2–CF_2 or CO_2–CF_3) and head segment–tail segment (CH_2CH_2O–CF_2 or CH_2CH_2OH–CF_3)].

Contact Energy Between Mutually Incompatible Molecular Units

We utilize the expression for the Gibbs energy of mixing, ΔG_{mix} given by the lattice fluid theory [17] and the double tangent construction [26] to calculate the solubility of the head segment [$(CH_2CH_2O)H$] in the solvent (CO_2). We vary χ_{ab} in ΔG_{mix} to approximately match this to the experimentally measured solubilities for ethanol in $scCO_2$ at $T = 350\,\mathrm{K}$ and supercritical pressures [27], resulting in $\chi_{sH} = 4.6$. The value of the solvent–head segment contact energy corresponding to this χ_{sH} [see Eqs. (1) and (2)] is: $\varepsilon_{sH}/k_{\mathrm{B}} = 0\,\mathrm{K}$.

Contact Energies Between Mutually Compatible Molecular Units

Applying the standard Berthelot combining rule to the calculation of unlike contact energies in our system does not automatically yield the correct sign for the Flory–Huggins interaction parameter χ_{ab} for mutually compatible molecular units. Therefore, we suggest the following modification of the standard Berthelot combining rule which takes into account the sign of χ_{ab}:

$$\varepsilon_{ab} = -\sqrt{\varepsilon^{*} \cdot \varepsilon^{\chi}} \tag{3}$$

where

$$\varepsilon^{*} = \frac{\varepsilon_{aa} + \varepsilon_{bb}}{2} \tag{4}$$

corresponds to a thermal solution ($\chi_{ab} = 0$) [18] and

$$\begin{aligned} \varepsilon^{\chi} &= \max(\varepsilon_{aa}, \varepsilon_{bb}) \quad \text{if } \chi_{ab} > 0 \\ &= \min(\varepsilon_{aa}, \varepsilon_{bb}) \quad \text{if } \chi_{ab} < 0 \end{aligned} \tag{5}$$

Use of this modified Berthelot combining rule therefore requires *a priori* knowledge of the sign of the Flory–Huggins interaction parameter and knowledge of like contact energies.

We assume only dispersion interactions between carbon dioxide and CF_2 or CF_3 groups as is suggested by the similar solubility parameters for $scCO_2$ and C_6F_{14} [27], and thus χ_{sT} must be small and positive. For interactions between the surfactant tail and head segments, we do not consider electrostatic or hydrogen bonding interactions and so assume that χ_{TH} is also positive.

All unlike contact energies and associated values for the Flory–Huggins interaction parameters at $T = 350\,\mathrm{K}$ are summarized in Table I.

Volume of Lattice Cell

To complete the description of the lattice model for the supercritical solvent–surfactant systems we need to specify the volume of a lattice cell v^* [17]. The lattice model assumes that the solvent molecules (CO_2), surfactant tail, (either a CF_2 or a CF_3 group) and head segments (either a CH_2CH_2O or a CH_2CH_2OH group) are all of the same size. This assumption is reasonable due to the similar size of the solvent molecules, and surfactant tail and head segments. Hence, we estimate a value for the volume of the lattice cell by matching the critical volume of the monomer lattice model fluid [22]: $\tilde{v}_{\mathrm{C}} \equiv v_{\mathrm{C}}/(\tilde{N}_{\mathrm{A}} v^{*}) = 2$ ($\tilde{N}_{\mathrm{A}}$ is the Avagadro's constant) with the experimental critical volume of carbon dioxide [21]: $v_{\mathrm{C}}^{\mathrm{CO_2}} = 94.12\,\mathrm{cm^3/mol}$, resulting in $v^{*} = 78.145\,\mathrm{\AA^3}$.

SIMULATION DETAILS

Methodology

Micellization is a single-phase phenomenon observed at low concentrations of surfactants but above the cmc. This necessitates the use of large-scale simulations; our lattices range in size from 50^3 (for higher surfactant concentrations) up to 220^3 (for lower surfactant concentrations) with periodic

boundary conditions. These large lattices allow us to have at least five to ten micelles present in the system at any one time. This number of micelles is sufficient enough to approximate the solution in the thermodynamic limit of infinite system size [28].

We carry out simulations at low surfactant concentrations for supercritical solvent conditions, and therefore the solvent molecules are the abundant species in the simulation box. To reduce CPU time we avoid explicit simulation of the solvent molecules by replacing them with "holes". The contact energies with the solvent molecules ε_{as} are set to zero and the rest of the contact energies are rescaled according to the values of the interchange energies w_{ab} defined by Eq. (1). Note that the contact energies with the vacancies become non-zero. Thus, only moves for the surfactants and vacancies need to be performed in the simulations.

The canonical (NVT) MC simulations utilize translation moves and particle interchanges for the monomeric species, and reptation moves and configurational-bias chain regrowth for the surfactants [29]. The simulations are organized in cycles. Each cycle consists of $N_v + rN_A$ attempts to move a randomly chosen particle; the type of move is selected randomly. Note that surfactant moves are attempted with higher frequency than monomeric moves to achieve better statistics. Configurational-bias and reptation moves are carried out with the same frequency. This scheme results in a very efficient sampling of configurational space. A typical MC run consists of 40,000–80,000 cycles for equilibration (starting from a random configuration) and 40,000 cycles for evaluation of the quantities of interest. CPU time requirements on a DEC Alpha 533 processor for a typical run are about 4 h/1000 cycles.

Characteristics of the Micellization Process

Several properties are calculated during the simulations in order to characterize the micellization process. These properties give information about the cmc and the size of the micelles. The computational definition of these quantities and the simulation criteria for existence of a micelle are described below.

Any surfactant that contains at least one head segment with a nearest or diagonally nearest neighbor contact to the head segment of another surfactant is considered to be part of a *micelle*. The aggregation number M is defined to be the number of surfactants contained in the micelle. Calculation of the aggregation number of the micelles is performed by the "cluster multiple labeling technique" of Hoshen and Kopelman [30]. Surfactants that are not part of micelles are referred to as *free unimers*.

Critical Micelle Concentration

Since there is no true phase transition between the non-aggregated and aggregated (micellar) states, the location of the cmc depends on the definition used [28]. We use Israelachvili *et al.*'s definition of the cmc as the concentration at which the number of surfactants aggregated in micelles is equal to the number of free unimers [31]. Other definitions of the cmc are related to a sharp change either in the solution osmotic pressure [32] or the polydispersity index, and/or to the first appearance of a peak in the aggregate size distribution as the surfactant concentration increases [33,34].

Micellar Size

To characterize the size of the spherical micelles we calculate the three principal radii of gyration [28,33]. The three principal radii of gyration, R_1, R_2, and R_3 (R_1 is the largest radius, followed by R_2 and then R_3) are the eigenvalues of the matrix of the radii of gyration. Elements of this matrix are defined to be

$$R_{\gamma\delta} = \left[\frac{1}{N_{\text{site}}}\sum_{i=1}^{N_{\text{site}}}(\gamma_i - \gamma_{\text{com}})(\delta_i - \delta_{\text{com}})\right]^{1/2} \tag{6}$$

where $\gamma_i, \delta_i \equiv x_i, y_i, z_i$ are the coordinates of surfactant segments in the micelle, $\gamma_{\text{com}}, \delta_{\text{com}} \equiv x_{\text{com}}, y_{\text{com}}, z_{\text{com}}$ are the coordinates of the center of mass of the micelle and N_{site} is the total number of surfactant segments in the micelle. For spherical micelles $R_1 \approx R_2 \approx R_3$.

MULTICOMPONENT SOLUTION MODEL

The multicomponent solution model is a conceptual framework that views a micellar solution as a multicomponent system consisting of solvent molecules, free unimers and aggregates of all possible sizes and shapes. Each of these aggregates is treated as a distinct chemical component [35,36]. The multicomponent solution model postulates a form for the free energy F which includes terms describing the essential physical factors responsible for the formation of micelles. These factors are: the entropy of mixing of the solvent molecules, free unimers and micelles F_m; the free-energy associated with the formation of individual micellar aggregates F_f; and the free energy of interaction between the solvent molecules, free unimers and micelles F_i. While the entropy of mixing given by the lattice fluid theory [17] can be used, for example, to calculate F_m, accurate calculation of F_f and F_i is very difficult due to the complexity of micellar solutions [35]. The entropic term F_m can be written

using the entropy of mixing given by the lattice fluid theory [17] as

$$\frac{F_m}{k_B T} = N_s \ln \Phi_s + \sum_{M=1}^{\infty} N_M \ln \Phi_M + N_s \left[\frac{1-\rho}{\rho} \ln(1-\rho) + \ln \rho \right] + \sum_{M=1}^{\infty} N_M \left[rM \frac{1-\rho}{\rho} \ln(1-\rho) + \ln \rho \right] \quad (7)$$

where ρ is the system density, N_M is the number of micelles with aggregation number M, Φ_s is the volume fraction of solvent molecules and Φ_M is the volume fraction of micelles with M. The quantities ρ, Φ_s, and Φ_M are defined to be

$$\rho = \frac{(N_s + rN_A)v^*}{V} = \frac{r\bar{N}_A v^*}{(r\Phi_s + \Phi_A)v}$$
$$\Phi_s = \frac{N_s}{N_s + rN_A} \quad \Phi_M = \frac{rMN_M}{N_s + rN_A} \quad (8)$$

respectively, where V is the system volume, v is the molar volume of the supercritical solvent–surfactant system and Φ_A is the surfactant volume fraction that is defined to be

$$\Phi_A = \frac{rN_A}{N_s + rN_A} \quad (9)$$

The standard-state F_f and the enthalpic F_i terms are typically expressed [35,36] as

$$F_f = N_s \mu_s^0 + \sum_{M=1}^{\infty} N_M \mu_M^0 \quad (10)$$

and

$$\frac{F_i}{k_B T} = N_s \ln \gamma_s + \sum_{M=1}^{\infty} N_M \ln \gamma_M \quad (11)$$

respectively. In Eqs. (10) and (11), μ_s^0 and μ_M^0 are the standard state chemical potentials of solvent molecules and micelles of size M, respectively, and γ_s and γ_M are the corresponding activity coefficients. The standard state for the solvent molecules is defined to be the pure solvent and the standard state for the micelles is the infinite dilute solution. Hence, the definition of the activity coefficients requires [37] that

$$\lim_{\Phi_A \to 0} \gamma_1 = \lim_{\Phi_A \to 0} \gamma_M = 1 \quad \forall\, M \quad (12)$$

At thermodynamic equilibrium, the chemical potential of surfactant must be the same whether the surfactant is in the form of free unimer or the part of a micelle, i.e.

$$\mu_1 = \frac{\mu_2}{2} = \frac{\mu_3}{3} = \ldots = \frac{\mu_M}{M} \quad (13)$$

where the chemical potential of a micelle of size M, μ_M, is calculated from $F = F_m + F_f + F_i$ as [26]

$$\mu_M \equiv \left(\frac{\partial F}{\partial N_M} \right)_{N_s, \{N_M^1\}, V, T} \quad (14)$$

From the equivalence of the chemical potential per surfactant of all micelles, Eq. (13), we obtain the following expression for the aggregate size distribution:

$$\Phi_M = \frac{\gamma_1^M}{\gamma_M} \Phi_1^M \exp[(M-1)(1 + \ln \rho)] \exp\left(-M \frac{\Delta\mu_M^0}{k_B T} \right) \quad (15)$$

where

$$\Delta\mu_M^0 = \frac{\mu_M^0}{M} - \mu_1^0 \quad (16)$$

is the standard state chemical potential difference. It should be mentioned that the activity coefficients γ_M are a function of system volume V, temperature T and surfactant volume fraction Φ_A, and the standard state chemical potential difference $\Delta\mu_M^0$ is a function of V, T and of the shape of the micelles. Additionally, the aggregate size distribution must satisfy the mass balance constraint:

$$\Phi_A = \sum_{M=1}^{\infty} \Phi_M \quad (17)$$

STANDARD STATE CHEMICAL POTENTIAL FOR SPHERICAL MICELLES

To go beyond general thermodynamic results, we need an explicit expression for the standard state chemical potential difference $\Delta\mu_M^0$. Various models for $\Delta\mu_M^0$ have appeared in the literature over the last two decades; for a review see Ref. [36]. The majority of the models have been derived using phenomenological approaches, which require experimental information to obtain the model parameters. Most of the existing models for $\Delta\mu_M^0$ deal primarily with incompressible water–surfactant systems, and therefore are not applicable to the formation of micelles in supercritical solvents. An exception is the model of Nagarajan and Ganesh [38,39] which was developed for incompressible systems but can be modified for compressible systems. We provide such a modification that is described below for the formation of

the spherical micelles in a supercritical solvent model using the modified Larson's lattice model.

To formulate an expression for $\Delta\mu_M^0$, the geometrical features of the micelles need to be specified. We assume that the micelles are spherical and contain a completely segregated spherical core made up of the surfactant H blocks. The surfactant T blocks and solvent molecules are assumed to be present in the spherical shell region surrounding the micellar core. The core and shell regions are regarded as being separated by an interface. The geometry of the spherical micelles is described by specifying the volume of the micellar core

$$V_{\text{core}} = \frac{4\pi}{3}R^3 = Mmv^* + N_v^{\text{core}}v^* \tag{18}$$

and the volume of the shell region

$$V_{\text{shell}} = \frac{4\pi}{3}[(R+D)^3 - R^3] \tag{19}$$

where R is the core radius, D is the shell thickness and N_v^{core} is the number of vacancies in the core. Instead of N_v^{core}, it is more convenient to work with the micellar core density which is defined to be

$$\rho^{\text{core}} = \frac{Mm}{Mm + N_v^{\text{core}}} \tag{20}$$

A complete description of the spherical micelle therefore requires values for R (or M), D and ρ^{core}.

The quantity $\Delta\mu_M^0$ represents the change in the standard state free energy when a singly dispersed surfactant H_mT_n in solution is transferred to a micelle with aggregation number M. By considering all changes accompanying the transfer of the surfactants from a singly dispersed state to a micellar aggregate, we derive an expression for $\Delta\mu_M^0$ for the case of spherical micelles. Firstly, when micelles form, the solvent incompatible H block is transferred from the solvent to the solvent-free micellar core. Associated with this transfer are changes in the state of dilution $(\Delta\mu_M^0)_{H,\text{dil}}$ and in the state of deformation $(\Delta\mu_M^0)_{H,\text{def}}$. Secondly, the solvent compatible T block is transferred from the solvent to the solvent penetrated shell region. This transfer also involves changes in the state of dilution $(\Delta\mu_M^0)_{T,\text{dil}}$ and in the state of deformation $(\Delta\mu_M^0)_{T,\text{def}}$. Thirdly, the formation of the micelle localizes H_mT_n in such a way that the H block is confined to the micellar core while the T block is confined to the shell region and this provides a localized entropic contribution $(\Delta\mu_M^0)_{\text{loc}}$. Finally, the formation of the micelles is accompanied by the creation of an interface and this is described by the contribution $(\Delta\mu_M^0)_{\text{int}}$. Therefore, $\Delta\mu_M^0$ is the sum of these six contributions

$$\Delta\mu_M^0 = (\Delta\mu_M^0)_{H,\text{dil}} + (\Delta\mu_M^0)_{H,\text{def}} + (\Delta\mu_M^0)_{T,\text{dil}} + (\Delta\mu_M^0)_{T,\text{def}} + (\Delta\mu_M^0)_{\text{loc}} + (\Delta\mu_M^0)_{\text{int}} \tag{21}$$

or alternatively

$$\Delta\mu_M^0 = (\Delta\mu_M^0)_{\text{core}} + (\Delta\mu_M^0)_{\text{shell}} + (\Delta\mu_M^0)_{\text{interface}} \tag{22}$$

where

$$\begin{aligned}(\Delta\mu_M^0)_{\text{core}} &= (\Delta\mu_M^0)_{H,\text{dil}} + (\Delta\mu_M^0)_{H,\text{def}}\\ (\Delta\mu_M^0)_{\text{shell}} &= (\Delta\mu_M^0)_{T,\text{dil}} + (\Delta\mu_M^0)_{T,\text{def}}\\ (\Delta\mu_M^0)_{\text{interface}} &= (\Delta\mu_M^0)_{\text{loc}} + (\Delta\mu_M^0)_{\text{int}}\end{aligned} \tag{23}$$

In Eq. (22), we group the contributions responsible for the formation of the core, shell and interface.

Change in the State of Dilution of the H Block

Within the micelle, the H block is confined to the micellar core region where it is in a state similar to that of pure H blocks. Therefore, a contribution to the $(\Delta\mu_M^0)_{H,\text{dil}}$ term from this state arises only from the entropy of mixing of pure H blocks and vacancies within the micellar core.

In the infinitely dilute reference condition, the solvent incompatible H block is in a collapsed state minimizing its interactions with the solvent. However, complete exclusion of the solvent molecules is not possible due to restrictions in chain folding. The collapsed state is considered to be a spherical monomolecular globule (g) containing the collapsed H block, N_s^g solvent molecules and N_v^g vacancies. The entropic and energetic changes associated with the removal of the H block from its infinitely dilute reference condition to a state of pure H blocks provide contributions to $(\Delta\mu_M^0)_{H,\text{dil}}$.

To calculate these contributions, we need to specify the spherical monomolecular globule as follows. The diameter of the monomolecular globule $2R_{\infty,H}$ is equal to the end-to-end distance of the H block. The volume of the monomolecular globule $V_{\infty,H}$ is computed in terms of the chain expansion parameter of the H block α_H and the unperturbed end-to-end distance of the H block $m^{1/2}v^{*1/3}$ as

$$V_{\infty,H} = \frac{4\pi}{3}R_{\infty,H}^3 = mv^* + N_s^g v^* + N_v^g v^* \tag{24}$$

where

$$2R_{\infty,H} = \alpha_H m^{1/2} v^{*1/3} \tag{25}$$

The method used to estimate the chain expansion parameter of the H block α_H is that suggested by de Gennes [40]. The α_H is expressed using Eq. (25) and the volume of the H block in the monomolecular globule

$$V_H = mv^* = \frac{4\pi}{3}R_{\infty,H}^3\rho^g\Phi_H^g \tag{26}$$

as

$$\alpha_H = \left(\frac{6}{\pi}\right)^{1/3} \rho^{g\,-1/3} \Phi_H^{g\,-1/3} m^{-1/6} \tag{27}$$

where ρ^g is the density of the monomolecular globule and Φ_H^g is the H block volume fraction inside the monomolecular globule. The method of de Gennes further assumes that the monomolecular globule is a distinct phase that coexists in osmotic equilibrium with the solvent region surrounding it. The osmotic pressure outside the monomolecular globule is zero because there are no H blocks in this solvent region. By equating the osmotic pressure given by the lattice fluid theory [17] to zero, we obtain an equation for Φ_H^g

$$\ln(1 - \Phi_H^g) + \left(1 - \frac{1}{m}\right)\Phi_H^g + \chi_{sH}\rho^g \Phi_H^{g\,2} = 0 \tag{28}$$

Equation (28) has two solutions in the interval $\langle 0, 1\rangle$ and the largest one gives the relevant value for calculation of α_H [40].

Further, the interface of the monomolecular globule disappears on micellization, this interfacial energy provides a contribution to $(\Delta\mu_M^0)_{H,\mathrm{dil}}$. This contribution can be written as the product of the surface area of the monomolecular globule and the interfacial tension between pure H segments and solvent, σ_{sH}.

Then, the $(\Delta\mu_M^0)_{H,\mathrm{dil}}$ term is calculated from the entropy of mixing of pure H blocks and vacancies within the micellar core minus three terms accounting for: (i) the entropic and (ii) the energetic changes associated with the removal of the H block from its infinitely dilute reference condition to a state of pure H blocks (written in the framework of the lattice fluid theory [17] for an isolated chain molecule); and (iii) the term corresponding to the interfacial energy:

$$\begin{aligned}\frac{(\Delta\mu_M^0)_{H,\mathrm{dil}}}{k_\mathrm{B}T} &= m\frac{1-\rho^{\mathrm{core}}}{\rho^{\mathrm{core}}}\ln(1-\rho^{\mathrm{core}}) \\ &\quad - N_s^g\left[\ln\Phi_s^g + \frac{1-\rho^g}{\rho^g}\ln(1-\rho^g) + \ln\rho^g\right] \\ &\quad - \chi_{sH}N_s^g\Phi_H^g\rho^g - 4\pi R_{\infty,H}^2\frac{\sigma_{sH}}{k_\mathrm{B}T}\Phi_H^g\end{aligned} \tag{29}$$

where

$$N_s^g = \frac{\rho^g V_{\infty,H} - m v^*}{v^*} \tag{30}$$

and Φ_s^g is the solvent volume fraction inside the monomolecular globule given as

$$\Phi_s^g = 1 - \Phi_H^g \tag{31}$$

The interfacial tension σ_{sH} can be estimated using the expression [41]

$$\sigma_{sH} = \left(\frac{k_\mathrm{B}T}{v^{*2/3}}\right)\left(\frac{\chi_{sH}}{6}\right)^{1/2} \tag{32}$$

Change in the State of Deformation of the H Block

Within the micellar core the H block is stretched over a length equal to the core radius R. The free energy of this deformation compared to the unperturbed end-to-end distance of the H block is estimated using the Flory model [19] for the deformation of a chain molecule along one direction, keeping the volume of the chain molecule constant. In the singly dispersed state of the H block, the deformation of the H block is characterized by the chain expansion parameter of the H block α_H and is written using the Flory expression [19] for an isolated chain molecule. The $(\Delta\mu_M^0)_{H,\mathrm{def}}$ term is then given as the difference between the free energy of the deformation of the H block within the micellar core and the free energy of the deformation of the H block in the singly dispersed state as

$$\begin{aligned}\frac{(\Delta\mu_M^0)_{H,\mathrm{def}}}{k_\mathrm{B}T} &= \left[\frac{1}{2}\left(\frac{R^2}{m v^{*2/3}} + 2\frac{m^{1/2}v^{*1/3}}{R} - 3\right)\right] \\ &\quad - \left[\frac{3}{2}(\alpha_H^2 - 1) - \ln\alpha_H^3\right]\end{aligned} \tag{33}$$

Change in the State of Dilution of the T Block

The $(\Delta\mu_M^0)_{T,\mathrm{dil}}$ term is estimated by following an approach parallel to that used for the H block. Within the micelle, the T block are present in the shell region. The shell region is considered to be equivalent to a chain network swollen by solvent molecules. Besides the T blocks the shell region contains N_s^{shell} solvent molecules and N_v^{shell} vacancies. The shell region provides entropic and energetic contributions to $(\Delta\mu_M^0)_{T,\mathrm{dil}}$.

In the singly dispersed state, the T block is swollen by solvent molecules. The swollen region of the T block (sw) is considered to be a sphere which also contains N_s^{sw} solvent molecules and N_v^{sw} vacancies. The swollen region of the T block provides entropic and energetic contributions to $(\Delta\mu_M^0)_{T,\mathrm{dil}}$.

To calculate these contributions, we need to specify the swollen region of the T block (considered to be a sphere) as follows. The diameter of the sphere $2R_{\infty,T}$ is equal to the end-to-end distance of the T block. The volume of the sphere $V_{\infty,T}$ is computed from the chain expansion parameter of the T block α_T

and the unperturbed end-to-end distance of the T block $n^{1/2}v^{*1/3}$ as

$$V_{\infty,T} = \frac{4\pi}{3}R_{\infty,T}^3 = nv^* + N_s^{sw}v^* + N_v^{sw}v^* \tag{34}$$

where

$$2R_{\infty,T} = \alpha_T n^{1/2} v^{*1/3} \tag{35}$$

The value of the chain expansion parameter of the T block α_T is estimated using the Flory expression [19,42] as

$$\alpha_T^5 - \alpha_T^3 = 0.88\left(\frac{1}{2} - \chi_{sT}\right)n^{1/2} \tag{36}$$

Then, the $(\Delta\mu_M^0)_{T,\text{dil}}$ term is equal to (i) the entropic and (ii) the energetic contributions resulting from the swelling of the T blocks by the solvent molecules in the shell region (written using the lattice fluid theory [17]) minus (iii) the entropic and (iv) the energetic contributions resulting from the swelling of the T block by the solvent molecules in the singly dispersed state (expressed in the framework of the lattice fluid theory [17] for an isolated chain molecule):

$$\begin{aligned}\frac{(\Delta\mu_M^0)_{T,\text{dil}}}{k_BT} = {} & \frac{1}{M}N_s^{\text{shell}}\left(\ln\Phi_s^{\text{shell}} + \frac{1-\rho^{\text{shell}}}{\rho^{\text{shell}}}\ln(1-\rho^{\text{shell}}) + \ln\rho^{\text{shell}}\right) \\ & + \frac{1}{M}\chi_{sT}N_s^{\text{shell}}\Phi_T^{\text{shell}}\rho^{\text{shell}} \\ & - N_s^{sw}\left[\ln\Phi_s^{sw} + \frac{1-\rho^{sw}}{\rho^{sw}}\ln(1-\rho^{sw}) + \ln\rho^{sw}\right] \\ & - \chi_{sT}N_s^{sw}\Phi_T^{sw}\rho^{sw}\end{aligned} \tag{37}$$

where

$$\begin{aligned}N_s^{\text{shell}} &= \frac{\rho^{\text{shell}}V_{\text{shell}} - Mnv^*}{v^*} \\ N_s^{sw} &= \frac{\rho^{sw}V_{\infty,T} - nv^*}{v^*}\end{aligned} \tag{38}$$

ρ^{shell} is the density in the shell region, ρ^{sw} is the density in the swollen region, Φ_s^{shell} is the solvent volume fraction in the shell region, Φ_T^{shell} is the T block volume fraction in the shell region, Φ_s^{sw} is the solvent volume fraction in the swollen region and Φ_T^{sw} is the T block volume fraction in the swollen region. The volume fractions Φ_s^{shell}, Φ_T^{shell}, Φ_s^{sw} and Φ_T^{sw} are defined to be

$$\begin{aligned}\Phi_s^{\text{shell}} &= \frac{\rho^{\text{shell}}V_{\text{shell}} - Mnv^*}{\rho^{\text{shell}}V_{\text{shell}}} \quad \Phi_T^{\text{shell}} = 1 - \Phi_s^{\text{shell}} \\ \Phi_s^{sw} &= \frac{\rho^{sw}V_{\infty,T} - nv^*}{\rho^{sw}V_{\infty,T}} \quad \Phi_T^{sw} = 1 - \Phi_s^{sw}\end{aligned} \tag{39}$$

Change in the State of Deformation of the T Block

Within the shell region the T block is stretched over a length equal to the shell thickness D. In analogy to the derivation of $(\Delta\mu_M^0)_{H,\text{def}}$, $(\Delta\mu_M^0)_{T,\text{def}}$ is given as the difference between the free energy of the deformation of the T block within the shell region and the free energy of the deformation of the T block in the singly dispersed state as

$$\begin{aligned}\frac{(\Delta\mu_M^0)_{T,\text{def}}}{k_BT} = {} & \left[\frac{1}{2}\left(\frac{D^2}{nv^{*2/3}} + 2\frac{n^{1/2}v^{*1/3}}{D} - 3\right)\right] \\ & - \left[\frac{3}{2}(\alpha_T^2 - 1) - \ln\alpha_T^3\right]\end{aligned} \tag{40}$$

Localization of the Surfactant Chain

The formation of micelles localizes the surfactant chain H_mT_n in such a way that the joint linking blocks H and T is constrained to the interfacial region. The entropic reduction associated with the localization is modeled using the concept of configurational volume restriction [38,39]. The $(\Delta\mu_M^0)_{\text{loc}}$ term is calculated as the ratio between the volume available to the joint linking blocks II and T in the interface and the total volume of the micelle:

$$\begin{aligned}\frac{(\Delta\mu_M^0)_{\text{loc}}}{k_BT} &= -\ln\left[\frac{4\pi R^2 v^{*1/3}}{(4\pi/3)(R+D)^3}\right] \\ &= -\ln\left[\frac{3R^2v^{*1/3}}{(R+D)^3}\right]\end{aligned} \tag{41}$$

Creation of the Interface

The formation of micelles is associated with the creation of the interface between the micellar core and the shell region. The $(\Delta\mu_M^0)_{\text{int}}$ term is estimated as the product of the surface area of the micellar core and an interfacial tension characterizing the interface. Since the shell region is dilute in T blocks, the interfacial tension is approximated to be σ_{sH} [38,39]. The $(\Delta\mu_M^0)_{\text{int}}$ term is calculated from

$$\frac{(\Delta\mu_M^0)_{\text{int}}}{k_BT} = \frac{4\pi R^2}{M}\frac{\sigma_{sH}}{k_BT} \tag{42}$$

RESULTS AND DISCUSSION

Lattice MC Simulations

We use three types of surfactant, H_4T_7, H_4T_{11} and H_6T_{11}, to study the effects of tail- and head-length variations on the micellar behavior in the lattice model systems of $scCO_2$–$F(CF_2)_n(CH_2CH_2O)_mH$. We carry out NVT MC simulations of the model supercritical solvent–surfactant systems at a reduced temperature $T_r \equiv T/T_C^{CO_2} = 1.15$, and reduced solvent densities, $\rho_r \equiv v_C^{CO_2}/v$, ranging from 1 to 1.82. At each simulated solvent density, the surfactant concentration is varied from $\Phi_A \approx 0.1\%$ to $\Phi_A \approx 8\%$. Typically, we perform two simulations below the cmc and four simulations above the cmc. At surfactant concentrations below the cmc, the aggregate size distribution exhibits only one peak, which represents unimers. At surfactant concentrations above the cmc, peaks in the aggregate size distribution form. These peaks and the principal radii of gyration are taken as criteria for the identification of micellar-type aggregates [28].

Since the simulations are carried out in the canonical ensemble, care must be taken to avoid simulating at state points that fall within an unstable region. If a state point lies within the unstable region, a peak in the aggregate size distribution may form. However, such a peak indicates the onset of the formation of an additional phase rather than the formation of a micellar aggregate. As the simulation box size increases, this peak will move towards higher aggregation numbers and become infinite in the thermodynamic limit. In contrast, micellar peaks should stay at approximately the same aggregation number as the simulation box size increases. Similarly, values of the principal radii of gyration characterizing the size and shape of micellar aggregates should be constant as the simulation box size increases since micelles of the same size and shape must form regardless of the size of the simulation box [28]. Hence, we check to ensure that we are outside an unstable region by repeating some simulations in a larger simulation box to determine if the aggregate size distribution and the principal radii of gyration are fixed. This check is typically performed for each simulated solvent density at the highest surfactant concentration studied. We usually increase the size of the simulation box by doubling the number of surfactants. We find that the H_4T_7 system at $\rho_r < 1.3$ does not form micelles but clusters of random shapes; this indicates an unstable region.

To determine the values of the cmc at various solvent densities, we plot the mole fraction of free unimers x_1 vs. surfactant mole fraction x_A as shown in Fig. 2. Below the cmc where there are no micelles and nearly all surfactants are in the form of free unimers, x_1 is equal to x_A and the simulation points therefore lie on the curve $x_1 = x_A$. Above the cmc, there is a region where x_1 is a decreasing linear function of x_A. The linear decrease in x_1 with increasing x_A has already been observed in previous simulations on Larson-type models [28,33,43–45].

We define the cmc as the surfactant mole fraction at which the number of surfactants aggregated in micelles is equal to the number of free unimers [31]. The value of the cmc at various ρ_r is determined as the point of intersection of the curve x_1 vs. x_A with the curve $x_1 = x_A/2$. Figure 3 shows values of the cmc expressed in volume fraction Φ_{cmc} vs. ρ_r. We see from Fig. 3 that the values of the cmc decrease with increasing ρ_r for the three surfactants studied. The cmc for the surfactant with more H segments, H_6T_{11}, is substantially lower than the cmc's for the surfactants with less H segments, H_4T_7 and H_4T_{11}. The cmc's for the surfactants with a fixed number of H segments but with a different number of T segments, H_4T_7 and H_4T_{11}, do not differ significantly from each other—the cmc for H_4T_{11} is only slightly higher than that for H_4T_7. The observed dependence of the cmc's on the number of H and T segments agrees with experimental observations for nonionic surfactants alkylpoly(ethylene oxide) in water where the cmc's increase with increasing poly(ethylene oxide) chain length and decrease with increasing alkyl chain length (see Figs. 15.15 and 15.16 in Ref. [36]).

Figure 4 displays a typical aggregate size distribution Φ_M vs. M at a state point below the cmc ($H_4T_{11} : T_r = 1.15,\ \rho_r = 1.400,\ \Phi_A = 1\%$). The aggregate size distribution exhibits only a unimeric peak and decays sharply to zero for $M > 1$. In Fig. 4, we also see that small fractions of dimers and trimers are formed.

Figure 5 presents a typical aggregate size distribution, and the three principal radii of gyration $\{R_1, R_2, R_3\}$ vs. M at a state point above the cmc ($H_4T_{11} : T_r = 1.15,\quad \rho_r = 1.718,\quad \Phi_A = 2.5\%$). The aggregate size distribution (Fig. 5a) displays a unimeric peak and a micellar peak at $M \approx 55$; the aggregate size distribution is symmetrical around the micellar peak. Similar values of the three principal radii of gyration (Fig. 5b) confirm that the system contains spherical micelles. A peak in R_1 at $M \approx 85$ has no physical significance (an artifact of simulation) since the aggregate size distribution is virtually zero here.

Multicomponent Solution Model

We combine the expression for the aggregate size distribution, Eq. (15), with the simulated aggregate size distributions to evaluate the standard state

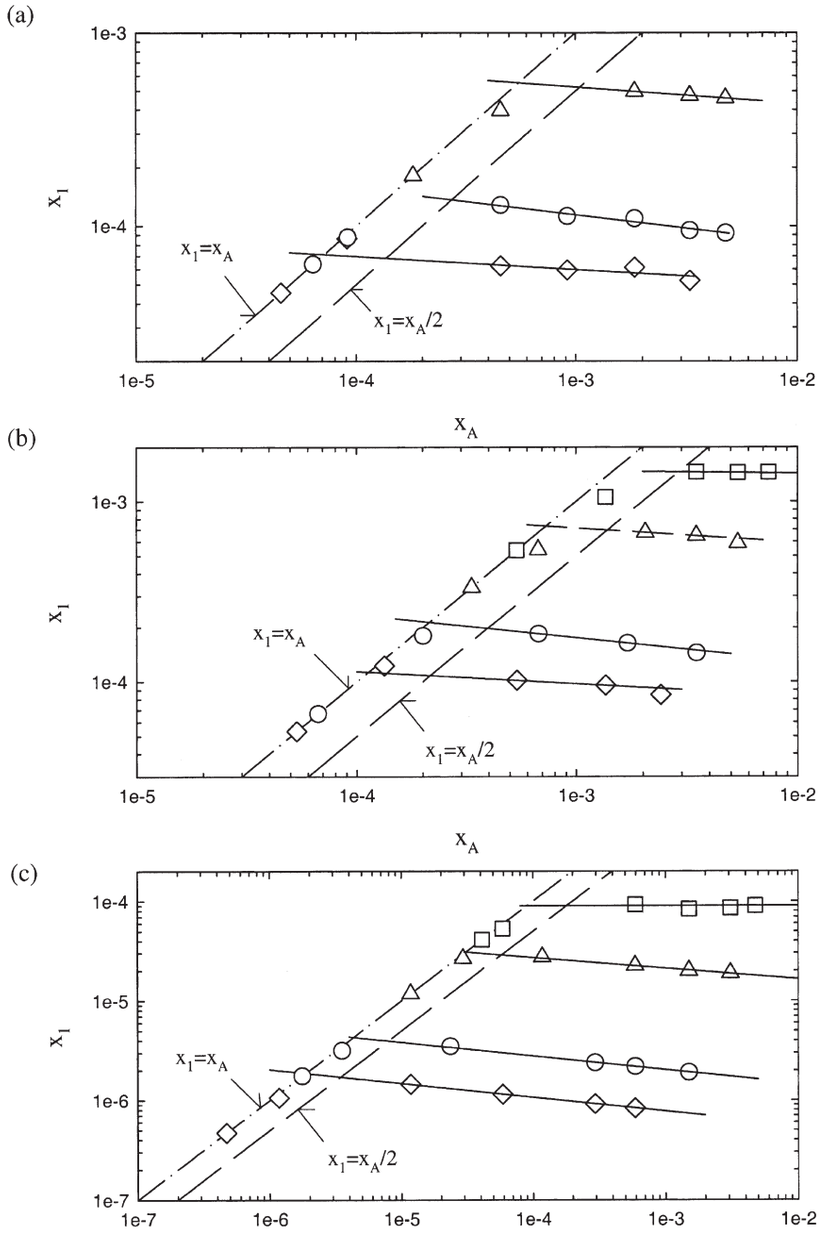

FIGURE 2 Mole fraction of the free unimers x_1 vs. surfactant mole fraction x_A for (a) H_4T_7, (b) H_4T_{11} and (c) H_6T_{11} in a supercritical solvent at a reduced temperature of 1.15 and reduced solvent densities $\rho_r = 1.000$ (□), 1.400 (△), 1.718 (○), and 1.818 (◇). The dashed line corresponds to $x_1 = x_A/2$, the dash–dotted line represents $x_1 = x_A$ and solid lines are fits of the simulation results.

chemical potential of micelles and the intermicellar interaction. We start by rewriting Eq. (15) in the form:

$$h(M, \Phi_A) \equiv \ln \Phi_1 - \frac{1}{M} \ln \Phi_M = \left(\frac{1}{M} \ln \gamma_M - \ln \gamma_1\right) - \frac{M-1}{M}(1 + \ln \rho) + \frac{\Delta\mu_M^0}{k_B T} \quad (43)$$

where Φ_1 and Φ_M are measured within the simulations for various Φ_A. Figure 6 shows an example of the h-function calculated for H_4T_{11} at $\rho_r = 1.400$ and $\Phi_A = 3$, 5 and 7.5%. Figure 6 clearly demonstrates the Φ_A-dependence of the h-function and also shows a shallow minimum in the h-function at an M corresponding to the position of the micellar peak in the aggregate size distributions. Since at constant V and T, γ_M is a function of Φ_A and $\Delta\mu_M^0$ does *not* depend on Φ_A, the values of $h(M, \Phi_A)$ at $\Phi_A = 0$ give values of the standard state chemical potentials $\Delta\mu_M^0$.

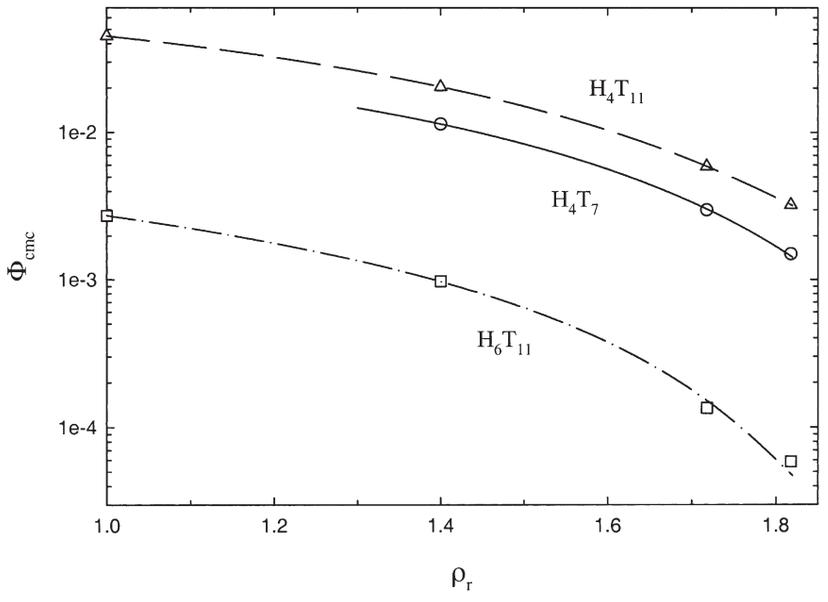

FIGURE 3 Critical micelle concentration expressed in volume fraction Φ_{cmc} vs. reduced solvent density ρ_r for H_4T_7 (○, —), H_4T_{11} (△, – – –) and H_6T_{11} (□, – · – · –) in a supercritical solvent at a reduced temperature of 1.15.

To proceed further, we need a functional form for $\ln \gamma_M$. Following Desplat and Care [44], we consider, as a first approximation, a linear dependence of $\ln \gamma_M$ on Φ_A:

$$\ln \gamma_M = a_M \Phi_A \quad \forall\ M \tag{44}$$

Note that Eq. (44) is valid only at low Φ_A and that it satisfies Eq. (12). Using Eq. (44), we may rewrite Eq. (43) as

$$h(M, \Phi_A) = \left(\frac{a_M}{M} - a_1\right)\Phi_A - \frac{M-1}{M}(1 + \ln \rho) + \frac{\Delta\mu_M^0}{k_B T} \tag{45}$$

By fitting the simulated aggregate size distributions to Eq. (45), we determine the intermicellar

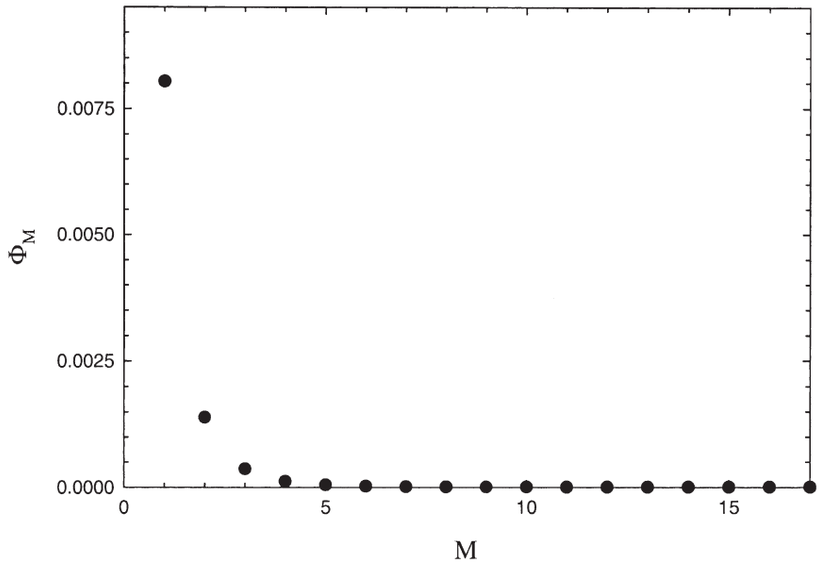

FIGURE 4 Aggregate size distribution plotted as the volume fraction of micelles of size M Φ_M vs. M below the cmc for vol% of H_4T_{11} in a supercritical solvent at a reduced temperature of 1.15 and a reduced solvent density of 1.400.

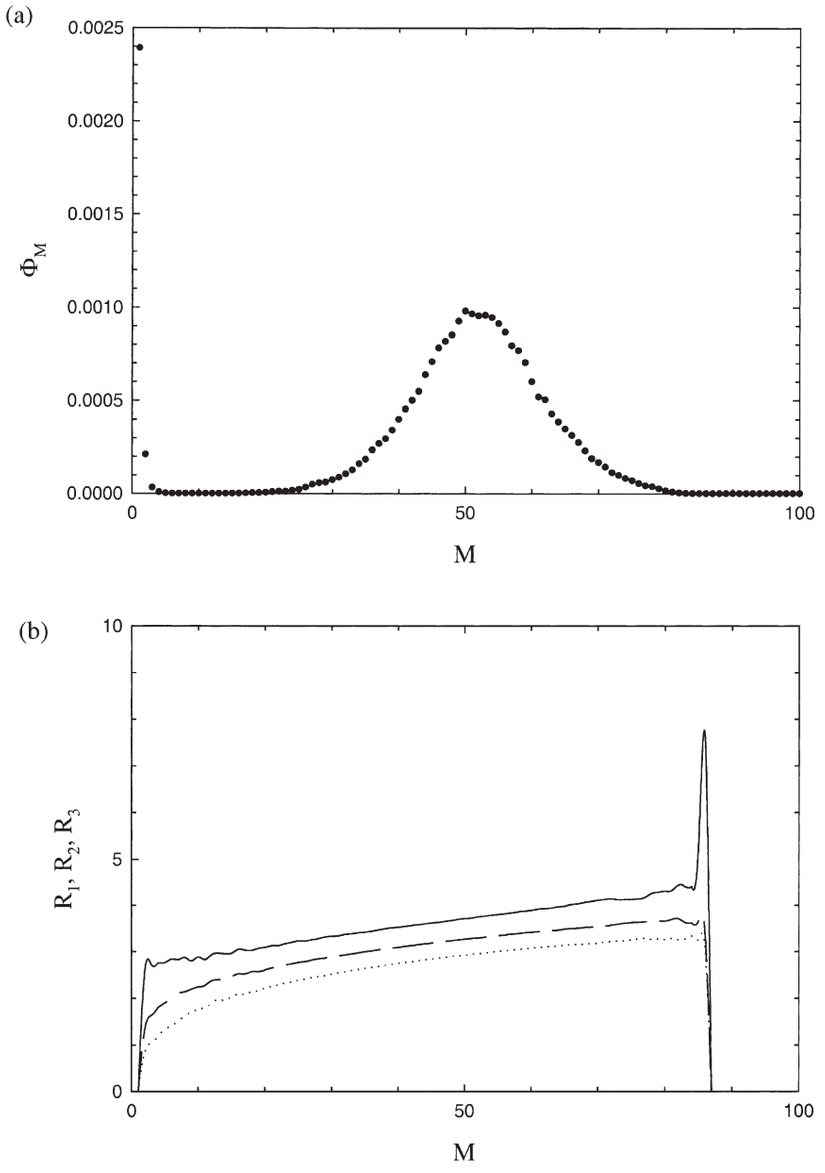

FIGURE 5 (a) Aggregate size distribution plotted as the volume fraction of micelles of size M Φ_M vs. M, and (b) three principal radii of gyration R_1 (—), R_2 (– – –), R_3 (·····) vs. M above the cmc for 2.5 vol% of H_4T_{11} in a supercritical solvent at a reduced temperature of 1.15 and a reduced solvent density of 1.718.

interaction characterized by the term $(a_M/M) - a_1$ and the values for $\Delta\mu^0_M$.

Figure 7 displays the values of $(a_M/M) - a_1$ as a function of aggregation number M obtained for the H_4T_{11} system at a reduced temperature $T_r = 1.15$ and different reduced solvent densities ρ_r. From Fig. 7, we see that values of $(a_M/M) - a_1$ are roughly constant for $M > 20$. This is also the case for the H_4T_7 and H_6T_{11} systems (data not shown). It suggests the following approximation

$$\frac{a_M}{M} - a_1 = C(V,T) \quad \forall\, M > 1 \tag{46}$$

where C is a constant determined as the arithmetic average of the $(a_M/M) - a_1$ values at $M > 20$.

Figure 8 presents C vs. ρ_r for the three systems studied. If we take the magnitude of C as a measure of the intermicellar interaction we see from Fig. 8 that for the systems studied, the intermicellar interaction increases with increasing ρ_r and that this increase is slower for the H_6T_{11} system than for the H_4T_7 and H_4T_{11} systems. Furthermore, the H_6T_{11} system exhibits stronger intermicellar interaction than the H_4T_7 and H_4T_{11} systems and the intermicellar interactions for the H_4T_7 and H_4T_{11} systems differ only slightly.

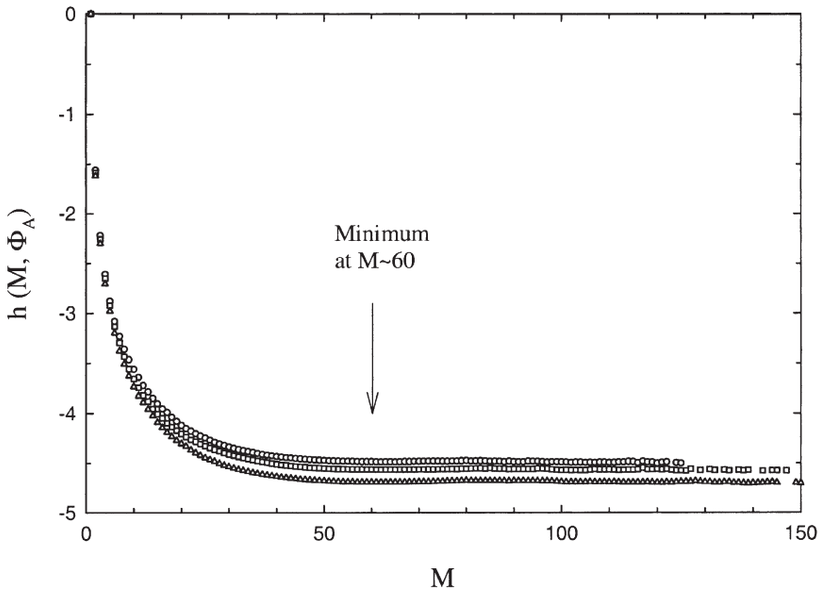

FIGURE 6 Function $h(M,\Phi_A)$, Eq. (43), for H_4T_{11} in a supercritical solvent at a reduced temperature of 1.15, a reduced solvent density of 1.400 and surfactant volume fractions $\Phi_A = 3\%$ (○), $\Phi_A = 5\%$ (□) and $\Phi_A = 7.5\%$ (△).

Figure 9 presents the values obtained for the standard state chemical potential difference $\Delta\mu_M^0$ vs. M (denoted by marks) for the H_4T_7, H_4T_{11} and H_6T_{11} systems at $T_r = 1.15$ and varying ρ_r. The quantity $\Delta\mu_M^0$ evaluated from simulation data is correlated using the modified Nagarajan–Ganesh model ("Standard state chemical potential for spherical micelles" section). Before proceeding with the correlation, we need to make additional simplifying assumptions about densities in the micellar core ρ^{core}, in the monomolecular globule ρ^g, in the shell region ρ^{shell} and in the swollen region ρ^{sw} to reduce the number of unknown variables. Due to the strong interaction between H blocks, we assume liquid-like density in the micellar core, i.e. $\rho^{core} \approx 1$. Furthermore, we approximate ρ^g, ρ^{shell} and ρ^{sw} from the density of pure solvent molecules, $\rho^g \approx \rho^{shell} \approx \rho^{sw} \approx \bar{N}_A v^*/v$, since the standard state for the micelles is an infinitely dilute solution. The only remaining independent variable is the shell thickness D which can be fit to simulation values for $\Delta\mu_M^0$ using equations given in "Standard state chemical

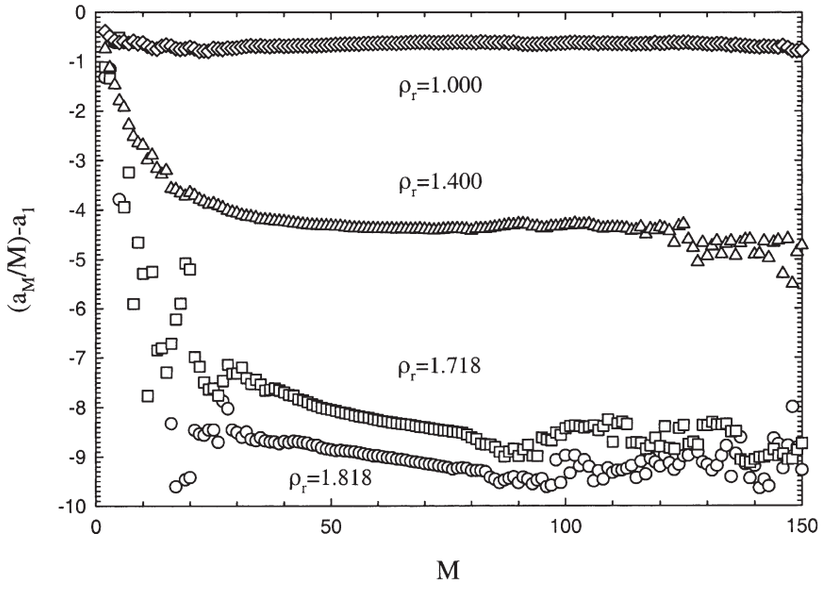

FIGURE 7 Intermicellar interaction term $a_M/M - a_1$, Eq. (45), vs. aggregation number M for H_4T_{11} in a supercritical solvent at a reduced temperature of 1.15 and reduced solvent densities $\rho_r = 1.000$ (◇), $\rho_r = 1.400$ (△), $\rho_r = 1.718$ (□) and $\rho_r = 1.818$ (○).

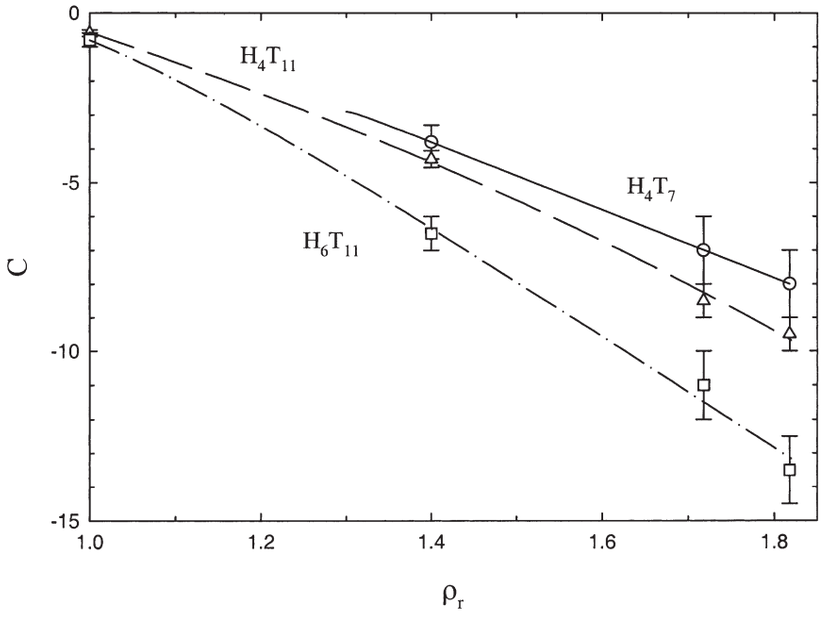

FIGURE 8 Intermicellar interaction C vs. reduced solvent density ρ_r for H_4T_7 (○, —), H_4T_{11} (△, – – –) and H_6T_{11} (□, – · – · –) in a supercritical solvent at a reduced temperature of 1.15.

potential for spherical micelles" section. As a result, we obtain the contributions to $\Delta\mu_M^0$ due to the micellar core $(\Delta\mu_M^0)_{\text{core}}$, shell region $(\Delta\mu_M^0)_{\text{shell}}$ and interface $(\Delta\mu_M^0)_{\text{interface}}$ together with the core radius R and shell thickness D. The contributions to $\Delta\mu_M^0$ are also shown in Fig. 9. From Fig. 9, we see that $\Delta\mu_M^0$ is negative and becomes more negative with increasing ρ_r. The term $(\Delta\mu_M^0)_{\text{core}}$ is also negative and becomes less negative with increasing ρ_r. The term $(\Delta\mu_M^0)_{\text{shell}}$ decreases with increasing ρ_r and has values close to zero for $\rho_r = 1.718$ and 1.818. The term $(\Delta\mu_M^0)_{\text{interface}}$ is positive and nearly insensitive to ρ_r.

Figure 10 displays predicted values for the core radius R and shell thickness D vs. M at $T_r = 1.15$ and varying ρ_r. Since we make the assumption that the density in the micellar core is liquid-like, the values of R do not depend on ρ_r. Figure 10 demonstrates the expected relation between the size of the core and shell regions and the number of H and T segments in the three surfactants studied. (The surfactants with more H and T segments form larger micellar cores and shell regions, respectively, than those with less H or T segments.) Figure 10 also shows that D increases with increasing ρ_r. This may be explained as follows. At high ρ_r where there are a lot of solvent molecules and only a few vacancies, the solvent compatible T segments maximize contacts with the solvent molecules. With decreasing ρ_r, the number of possible contacts of the T segments with the solvent molecules decreases since the number of vacancies in the system increases. Hence, T blocks are more stretched at higher ρ_r than at lower ρ_r resulting in an increase in D with increasing ρ_r.

We may interpret the micellization tendency of the H_4T_7, H_4T_{11} and H_6T_{11} systems in terms of $\Delta\mu_M^0$ and its contributions $(\Delta\mu_M^0)_{\text{core}}$, $(\Delta\mu_M^0)_{\text{shell}}$ and $(\Delta\mu_M^0)_{\text{interface}}$. For micellar formation to occur, $\Delta\mu_M^0$ must be negative [38]. From Fig. 9, we may therefore conclude that: (i) the micellization tendency increases with increasing ρ_r since $\Delta\mu_M^0$ becomes more negative with increasing ρ_r; (ii) the micellization tendency is stronger for the H_6T_{11} system than for the H_4T_7 and H_4T_{11} systems since $\Delta\mu_M^0$ for the H_6T_{11} system is more negative than $\Delta\mu_M^0$ for the H_4T_7 and H_4T_{11} systems; and (iii) the micellization tendency for the H_4T_7 and H_4T_{11} systems is very similar due to their similar $\Delta\mu_M^0$. The $(\Delta\mu_M^0)_{\text{core}}$ term provides the driving force for micellization. The incompatibility of the H segments with solvent molecules thus promotes micellization. However, the mutual incompatibility of the H and T blocks is also essential for micellization. Otherwise, the incompatibility of the H segments with the solvent molecules would merely lead to a macroscopic separation. The mutual incompatibility between the H and T blocks is implicitly taken into account by the completely segregated micellar core. Figure 9 clearly demonstrates the importance of the mutual incompatibility between the H and T blocks on the $(\Delta\mu_M^0)_{\text{core}}$ and $(\Delta\mu_M^0)_{\text{shell}}$ terms. The increase in D with increasing ρ_r (see Fig. 10) gives rise to a decrease in $(\Delta\mu_M^0)_{\text{shell}}$. This decrease is opposed by $(\Delta\mu_M^0)_{\text{core}}$ and this $(\Delta\mu_M^0)_{\text{core}}$ becomes less negative with increasing ρ_r.

Finally, Fig. 11 presents a typical example of the predictions using the multicomponent solution model for (a) the change in the number of free

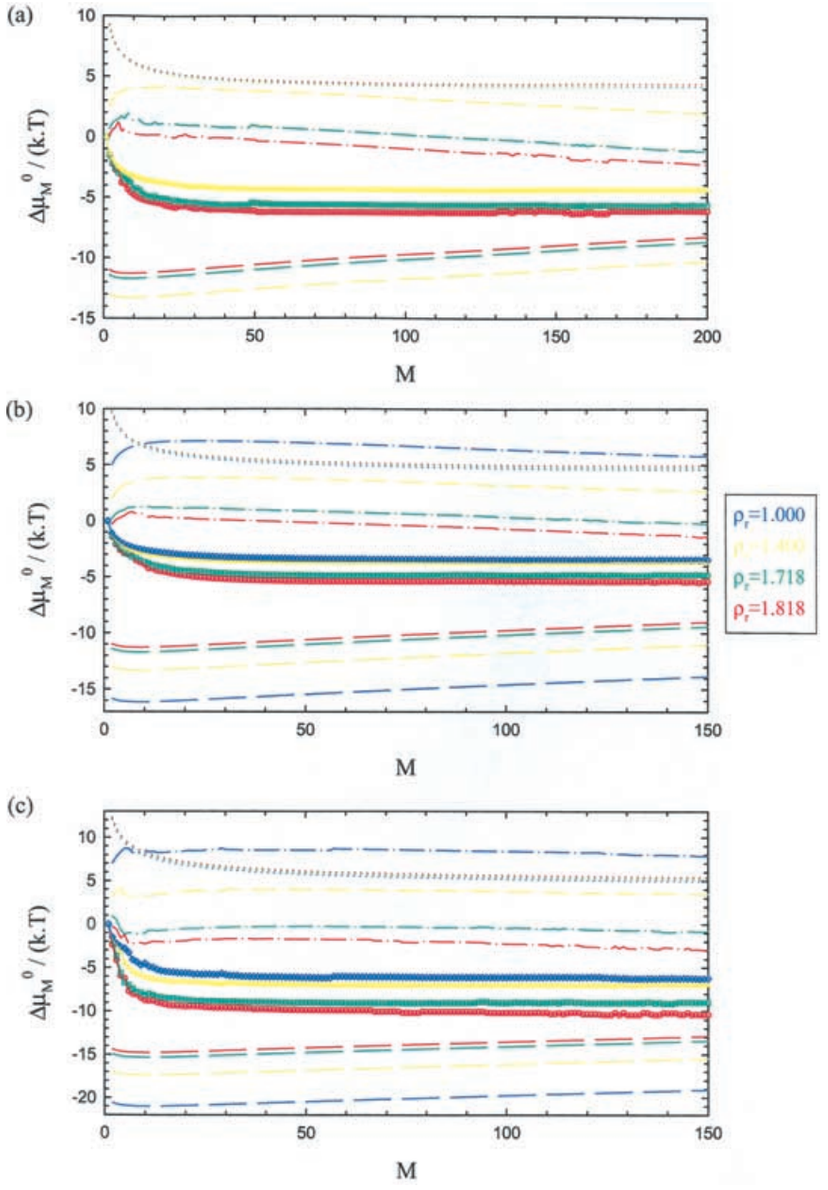

FIGURE 9 Standard state chemical potential difference $\Delta\mu_M^0$ vs. aggregation number M for (a) H_4T_7, (b) H_4T_{11} and (c) H_6T_{11} in a supercritical solvent at a reduced temperature of 1.15 and different reduced solvent densities ρ_r; T is the temperature and k_B is Boltzmann's constant. Circles, boxes, triangles and diamonds correspond to simulation values for $\Delta\mu_M^0$ at $\rho_r = 1.000$, 1.400, 1.718 and 1.818, respectively. The solid lines correspond to the correlation of simulated $\Delta\mu_M^0$ by means of the modified Nagarajan–Ganesh model. The dashed lines, dash–dotted lines and dotted lines represent contributions to $\Delta\mu_M^0$ from micellar core, shell region and interface, respectively, as predicted by the modified Nagarajan–Ganesh model.

unimers with surfactant concentration and (b) the change in the aggregate size distribution with Φ_A for H_4T_{11} system at $T_r = 1.15$ and $\rho_r = 1.400$. We calculate the volume fraction of the free unimers Φ_1 as a function of Φ_A above the cmc using Eqs. (17) and (45) and compare the predicted values of Φ_1 with simulation results in Fig. 11a. We see excellent agreement between simulated and predicted values of Φ_1. In Fig. 11a, we also show the predicted Φ_1 using multicomponent solution model with the intermicellar interaction switched off (C is set to zero). We see that in contrast to the simulation results, Φ_1 changes only slightly with increasing Φ_A. Therefore, we conclude that the decrease in Φ_1 with increasing Φ_A observed in our simulations as well as in previous simulations of Larson's model [28,33,43–45] is a consequence of the intermicellar interactions. Agreement between the simulated and predicted aggregate size distributions (Fig. 11b) is very good, especially at low Φ_A. The predicted position of the micellar peak is at a lower M than the simulation results. However, it should be noted that evaluating

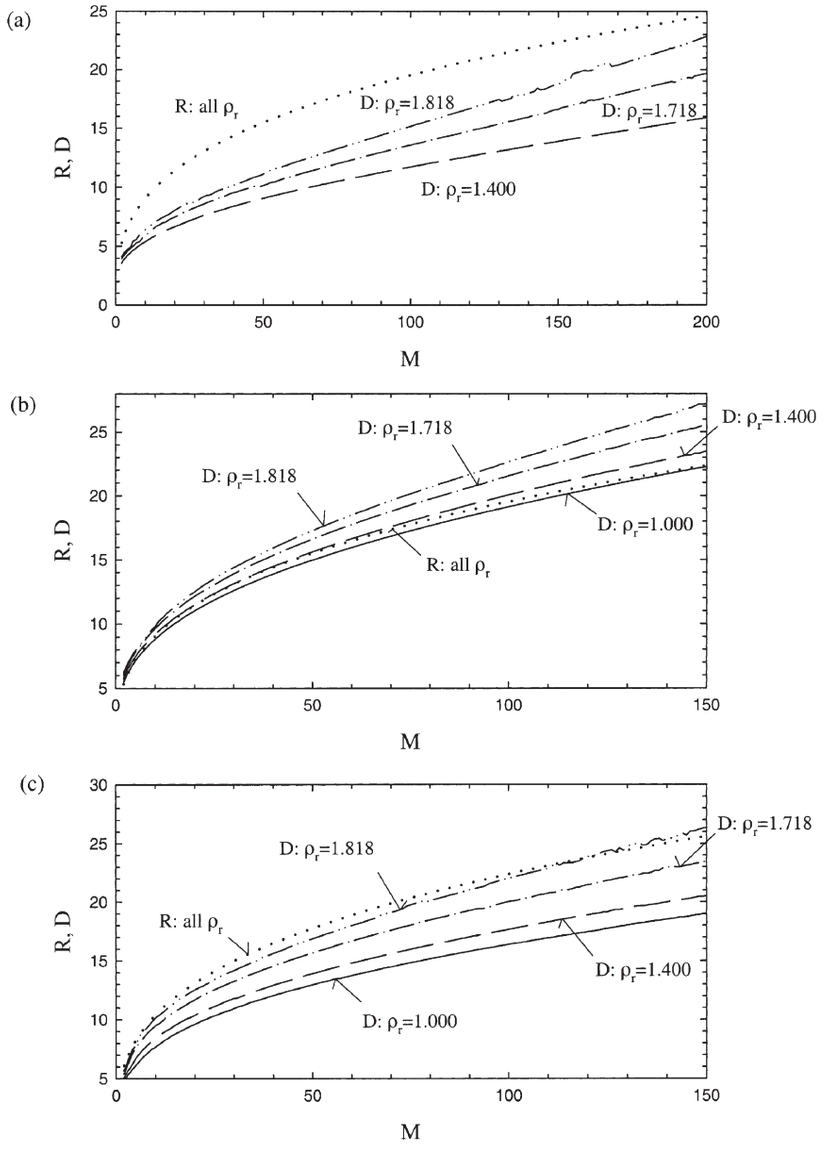

FIGURE 10 Core radius R and shell thickness D vs. aggregation number M for (a) H_4T_7, (b) H_4T_{11}, and (c) H_6T_{11} in a supercritical solvent at a reduced temperature of 1.15 and different reduced solvent densities ρ_r as predicted by the modified Nagarajan–Ganesh model. The dotted line represents values of R which are density independent. The solid, dashed, dash–dotted and dash–double-dotted lines correspond to values of D for $\rho_r = 1.000$, 1.400, 1.718 and 1.818, respectively.

$\Delta\mu_M^0$ from simulations is subject to uncertainties. Small errors in $\Delta\mu_M^0$ yield large discrepancies in the aggregate size distributions since $\Delta\mu_M^0$ appears in the exponent in Eq. (15).

CONCLUSIONS

We have studied self-assembly of a nonionic surfactant, perfluoroalkylpoly(ethylene oxide): $F(CF_2)_n(CH_2CH_2O)_mH$ ($m = 4–9$, $n = 7–11$; $m < n$) in $scCO_2$ using a modified version of Larson's lattice model, focusing on H_4T_7, H_4T_{11} and H_6T_{11} to observe the effect of tail- and head-length variations. We performed canonical MC simulations at the reduced temperature T_r of 1.15, varying the reduced solvent densities ρ_r from 1 to 1.82 and the surfactant volume fractions Φ_A from 0.1 to 8 vol%. At each simulation state point, we calculated the aggregate size distribution and the three principal radii of gyration. The cmc was determined as the concentration at which the number of surfactants aggregated in micelles is equal to the number of free unimers [31]. We found that the cmc for the surfactant with more H segments, H_6T_{11}, was substantially lower than the cmc's for the surfactants with less H segments, H_4T_7 and H_4T_{11}. The cmc's for the surfactants with a fixed number of H segments but with different T segments,

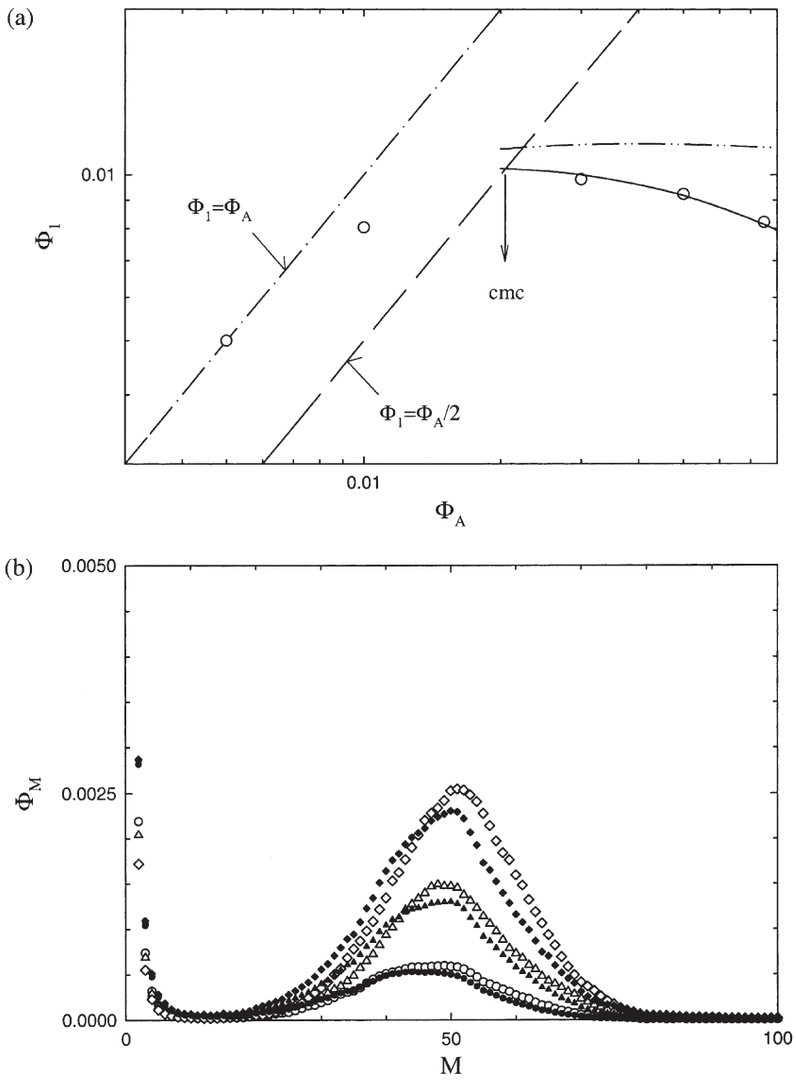

FIGURE 11 (a) Volume fraction of the free unimers Φ_1 vs. surfactant volume fraction Φ_A for H_4T_{11}, in a supercritical solvent at a reduced temperature of 1.15 and reduced solvent density of 1.400. Open circles represent simulation points. The dashed line corresponds to $\Phi_1 = \Phi_A/2$ and the dash–dotted line represents $\Phi_1 = \Phi_A$. The solid line is the prediction by means of the multicomponent solution model and the dash–double-dotted line is the calculation using the multicomponent solution model when the intermicellar interaction is switched off. (b) Aggregate size distribution plotted as the volume fraction of micelles of size M Φ_M vs. M for surfactant volume fractions $\Phi_A = 3\%$ (circles), $\Phi_A = 5\%$ (triangles) and $\Phi_A = 7.5\%$ (diamonds) of H_4T_{11} in a supercritical solvent at a reduced temperature of 1.15 and a reduced solvent density of 1.400. The open marks correspond to simulation results and filled marks represent predictions using the multicomponent solution model.

H_4T_7 and H_4T_{11}, did not differ significantly from each other. Further, we observed that the cmc's for the three systems studied decreased with increasing solvent density.

Finally, we used the multicomponent solution model in combination with the simulation results and determined the standard state chemical potential difference $\Delta\mu_M^0$ and the intermicellar interaction. We have modified the Nagarajan–Ganesh model for the standard state chemical potential and used it to correlate the values for $\Delta\mu_M^0$. From the correlation, we obtained $\Delta\mu_M^0$ contributions responsible for the formation of the micellar core, shell and interface as well as the micellar core radius and shell thickness. We found that: (i) the micellization tendency increased with increasing solvent density; (ii) the micellization tendency was stronger for the H_6T_{11} system than for the H_4T_7 and H_4T_{11} systems; and (iii) the micellization tendency for the H_4T_7 and H_4T_{11} systems was very similar due to their similar $\Delta\mu_M^0$.

Acknowledgements

The material is based upon work supported by the STC Program of the National Science Foundation under Agreement No. CHE-9876674 and by

the Grant Agency of the Czech Republic (Grants No. 203/00/0600 and No. 203/02/0805). ML thanks Flor R. Siperstein for fruitful discussions and many valuable comments.

References

[1] McHugh, M. and Krukonis, V. (1986) *Supercritical Fluid Extraction* (Butterworths, Boston, MA).

[2] DeSimone, J.M., Guan, Z. and Elsbernd, C.S. (1992) "Synthesis of fluoropolymers in supercritical carbon dioxide", *Science* **257**, 945–947.

[3] NSF Science and Technology Center, *Environmentally Responsible Solvents and Processes*, http://www.nsfstc.unc.edu.

[4] Yee, G.G., Fulton, J.L. and Smith, R.D. (1992) "Fourier transform infrared spectroscopy of molecular interactions of heptafluoro-1-butanol or 1-butanol in supercritical carbon dioxide and supercritical ethane", *J. Phys. Chem.* **96**, 6172–6181.

[5] Iezzi, A., Bendale, P., Enick, R.M., Turberg, M. and Brady, J. (1989) "Gel formation in carbon dioxide-semifluorinated alkane mixtures and phase equilibria of a carbon dioxide-perfluorinated alkane mixtures", *Fluid Phase Equilib.* **52**, 307–317.

[6] Salaniwal, S., Cui, S.T., Cummings, P.T. and Cochran, H.D. (1999) "Self-assembly of reverse micelles in water/surfactant/carbon dioxide systems by molecular simulation", *Langmuir* **15**, 5188–5192.

[7] Salaniwal, S., Cui, S.T., Cochran, H.D. and Cummings, P.T. (2000) "Molecular dynamics simulation of reverse micelles in supercritical carbon dioxide", *Ind. Eng. Chem. Res.* **39**, 4543–4554.

[8] Salaniwal, S., Cui, S.T., Cochran, H.D. and Cummings, P.T. (2001) "Molecular simulation of a dichain surfactant/water/carbon dioxide system. 1. Structural properties of aggregates. 2. Self assembly and aggregation dynamics", *Langmuir* **17**, 1773–1792.

[9] Baysal, C., Erman, B. and Chu, B. (2001) "Conformational features of Poly(1,1-dihydroperfluorooctyl acrylate) and poly(vinyl acctate) diblock oligomers in supercritical carbon dioxide", *J. Chem. Phys.* **114**, 5444–5449.

[10] Luna-Bárcenas, G., Mawson, S., Takishima, S., DeSimone, J.M., Sanchez, I.C. and Johnston, K.P. (1998) "Phase behavior of poly(1,1-dihydroperfluorooctyl acrylate) in supercritical carbon", *Fluid Phase Equilib.* **146**, 325–337.

[11] Chapman, W.G., Gubbins, K.E., Jackson, G. and Radosz, M. (1990) "New reference equation of state for associating liquids", *Ind. Eng. Chem. Res.* **29**, 1709–1721.

[12] Colina, C.M., Hall, C.K. and Gubbins, K.E. (2001) "Phase behavior of PVAC–PTAN block copolymer in supercritical carbon dioxide using SAFT", *Fluid Phase Equilib.*, in press.

[13] Shelley, J.C. and Shelley, M.Y. (2000) "Computer simulation of surfactant solutions", *Curr. Opin. Colloid Interface Sci.* **5**, 101–110.

[14] Larson, R.G., Seriven, L.E. and Davis, H.T. (1985) "Monte Carlo simulation of model amphiphile–oil–water systems", *J. Chem. Phys.* **83**, 2411–2420.

[15] Larson, R.G. (1996) "Monte Carlo simulations of the phase behavior of surfactant solutions", *J. Phys. II France* **6**, 1441–1463.

[16] Fulton, J.L., Pfund, D.M., McClain, J.B., Romack, T.J., Maury, E.E., Combes, J.R., Samulski, E.T., DeSimone, J.M. and Capel, M. (1995) "Aggregation of amphiphilic molecules in supercritical carbon dioxide: a small angle X-ray scattering study", *Langmuir* **11**, 4241–4249.

[17] Sanchez, I.A. and Panayiotou, C.G. (1994) "Equations of state thermodynamics of polymer and related solutions", In: Sandler, S.I., ed, *Models for Thermodynamic and Phase Equilibria Calculations* (Marcel Dekker, New York, NY).

[18] Tompa, H. (1956) *Polymer Mixtures* (Butterworths, London, UK).

[19] Flory, P.J. (1953) *Principles of Polymer Chemistry* (Cornell University Press, New York, NY).

[20] Rappé, A.K., Casewit, C.J., Colwell, K.S., Goddard, III, W.A. and Skiff, W.M. (1992) "UFF, a full periodic table force field for molecular mechanics and molecular dynamics simulations", *J. Am. Chem. Soc.* **114**, 10024–10035.

[21] Reid, R.C., Prausnitz, J.M. and Poling, B.E. (1987) *The Properties of Gases and Liquids* (McGraw-Hill, New York, NY).

[22] Mackie, A.D., Panagiotopoulos, A.Z. and Kumar, S.K. (1995) "Monte Carlo simulations of phase equilibria for a lattice homopolymer model", *J. Chem. Phys.* **102**, 1014–1023.

[23] Allen, M.P. and Tildesley, D.J. (1987) *Computer Simulation of Liquids* (Clarendon Press, Oxford, UK).

[24] Bates, F.S. and Fredrickson, G.H. (1999) "Block copolymers-designer soft materials", *Phys. Today* **Feb**, 32–38.

[25] Bates, F.S. (1991) "Polymer–polymer phase behavior", *Science* **251**, 898–905.

[26] Smith, J.M., Van Ness, H.C. and Abbott, M.M. (1996) *Introduction to Chemical Engineering Thermodynamics* (McGraw-Hill, New York, NY).

[27] Barton, A.F.M. (1983) *CRC Handbook of Solubility Parameters and Other Cohesion Parameters* (CRC Press, Boca Raton, FL).

[28] Mackie, A.D., Panagiotopoulos, A.Z. and Szleifer, I. (1997) "Aggregation behavior of a lattice model for amphiphiles", *Langmuir* **13**, 5022–5031.

[29] Frenkel, D. and Smit, B. (1996) *Understanding Molecular Simulation: From Algorithms to Applications* (Academic Press, London, UK).

[30] Hoshen, J. and Kopelman, R. (1976) "Percolation and cluster distribution I. Cluster multiple labeling technique and critical concentration algorithm", *Phys. Rev. B* **14**, 3438–3445.

[31] Israelachvili, J.N., Mitchell, D.J and Ninham, B.W. (1976) "Theory of self-assembly of hydrocarbon amphiphiles into micelles and bilayers", *J. Chem. Soc. Faraday Trans.* **2**(72), 1525–1568.

[32] Floriano, M.A., Caponetti, E. and Panagiotopoulos, A.Z. (1999) "Micellization in model surfactant systems", *Langmuir* **15**, 3143–3151.

[33] Talsania, S.K., Wang, Y., Rajagopalan, R. and Mohanty, K.K. (1997) "Monte Carlo simulations for micellar encapsulation", *J. Colloid Interface Sci.* **190**, 92–103.

[34] Talsania, S.K., Rodríguez-Guadarrama, L.A., Mohanty, K.K. and Rajagopalan, R. (1998) "Phase behavior and solubilization in surfactant–solute–solvent systems by Monte Carlo simulations", *Langmuir* **14**, 2684–2692.

[35] Ben-Shaul, A. and Gelbart, W.M. (1994) "Statistical thermodynamics of amphiphile self-assembly: structure and phase transitions in micellar solutions", In: Gelbart, W.M., Ben-Shaul, A. and Roux, D., eds, *Micelles, Membranes, Microemulsions and Monolayers* (Springer, New York, NY).

[36] Nagarajan, R. and Ruckenstein, E. (2000) "Self-assembled systems", In: Sengers, J.V., Kayser, R.F., Peters, C.J. and White, Jr, H.J., eds, *Equations of State for Fluids and Fluid Mixtures* (Elsevier, Amsterdam, The Netherlands).

[37] Tester, J.W. and Modell, M. (1996) *Thermodynamics and Its Applications* (Prentice Hall Inc., New Jersey, NJ).

[38] Nagarajan, R. and Ganesh, K. (1989) "Block copolymer self-assembly in selective solvents: spherical micelles with segregated cores", *J. Chem. Phys.* **90**, 5843–5856.

[39] Nagarajan, R. and Ganesh, K. (1989) "Block copolymer self-assembly in selective solvents: theory of solubilization in spherical micelles", *Macromolecules* **22**, 4312–4325.

[40] de Gennes, P.G. (1979) *Scaling Concepts in Polymer Physics* (Cornell University Press, New York, NY).

[41] Helfand, E. and Tagami, Y. (1971) "Theory of the interface between immiscible polymers", *J. Polym. Sci. B* **9**, 741–746.

[42] Stockmayer, W.H. (1955) "Chain dimensions near the Flory temperature", *J. Polym. Sci.* **15**, 595–597.

[43] Rodríguez-Guadarrama, L.A., Talsania, S.K., Mohanty, K.K. and Rajagopalan, R. (1999) "Thermodynamics of aggregation of amphiphiles in solution from lattice Monte Carlo simulations", *Langmuir* **15**, 437–446.

[44] Desplat, J.C. and Care, C.M. (1996) "A Monte Carlo simulation of the micellar phase of an amphiphile and solvent mixture", *Mol. Phys.* **87**, 441–453.

[45] Girardi, M. and Figueiredo, W. (2000) "Transition in three-dimensional micellar systems", *J. Chem. Phys.* **112**, 4833–4835.